Uses of WorldView-2 Multispectral Data in Extracting Potential Iron Mineralization Zones

Min Yang[1, a], Jianqiang Li[1, b] , Ting Gao[1,c], Guangli Ren[1,d], and Haihui Han[1, e]

[1]Xi'an Center of China Geological Survey, Xi'an 710054, China;

[a]mysteryyoung@qq.com, [b]405739307@qq.com, [c]orange_gt8212@sina.com, [d]renguangli9977@163.com [e]32742033@qq.com

Keywords: Spectral Matched Filtering, multispectral data, WorldView-2, iron oxide minerals mapping.

Abstract. A test site in West Kunlun area, China has been established to study the applications of WorldView-2 multispectral data to iron oxide minerals mapping. An iron oxide minerals distribution map was mapped by Spectral Matched Filtering (SMF) technique after the image data had been processed by atmospheric correction. The Gothite spectrum from USGS spectral library was chosen as the iron oxide mineral end member. And acoording to the result of SMF, field work was carried out and two potential iron minerlization zones were found in the study area. The study indicate that SMF method for WorldView-2 multispectral data holds promise for iron oxide minerals mapping in some iron ore deposits. And further analysis is required in different geologic environments in West Kunlun area to validate WorldView-2 multispectral data as a useful aid to land surface mapping.

1. Introduction

Reflectance spectroscopy is the study of solar light as a function of wavelength that has been emitted, reflected or scattered from a solid, liquid or gas [1]. The 0.4—1.0 μm wavelength region provides abundance mineral information based on analysis of electronic absorption features in transitional metals, especially iron oxide and other functional groups [2]. Imaging spectrometers carrying on the satellites provide a unique images of the Earth's surface unavailable from other sorces [3]. Imaging spectrometry data can be used to identify and map the spatial distribution of minerals based on the analysis of the spectroscopic information recorded in each image pixel. However, the identification of surface minerals from imaging spectrometer data is complicated by spectral unmixing. For the past decades, spectral unmixing methods have been evolving in step with the evolution of data collection systems [4].

To resolve the problem of the mixed pixel, the Spectral Matched Filter [SMF] of imaging spectrometer data has been described by Harsanyi and Chang [5]. The technique is a unique approach to spectral mixture modelling in that it does not require knowledge of the spectral signatures of other component, and in which only userchosen targets are mapped. In SMF, a spectrum is modelled as the sum of 'pure spectra' called end members. The simple SMF uses a fixed set of endmembers to decompose each image pixel. Unlike other unmixing methods, we don't need to find the spectra of all endmembers in the scene to get an accurate analysis. Spectral Matched Filtering was originally developed to compute abundances of targets that are relatively rare in the scene. SMF 'filters' the imput image for good matches to the chosen target spectrum by maximizing the response of the target spectrum within the data and suppressing the response of everything else. Applications of SMF include planetary mapping [5], plant species mapping [6], vegetation mapping [7-9], landform mapping [10-12], weak gas plumes detection [13], etc.

2. Study area

The study area is located on the banded iron formation belt in Xinjiang province, western China [Figure 1]. It has great potential for iron deposits exploration using remote sensing instruments.

According to Zhengwei Zhang[14], the west Kunlun Mountains are one of the largest potential districts for searching large and super large scale metallogenic ore deposits in western China and have attracted domestic and international attention [15]. The Mountains located to the northwestern Tibetan Plateau [also called as Qinghai-Tibet Plateau] and to the southwestern Tarim Basin, are very important in regional tectonic geology in China and central Asia. Tectonically, this area is also one part of the Kunlun orogenic zone, being situated between the ancient Asian structural field and the Tethyan structural field. Associated with the distribution of tectonic zones, there are several huge ore-forming zones passing through the west Kunlun Mountains such as the Kunlun-Qilian-Qinling ore-forming zone, Sanjiang ore-forming zone and middle Asia ore-forming zone [16]. The Sanjiang zone is named to indicate three rivers; the Jinshajiang River, the Lancangjiang River and the Nujiang River, and these three rivers originate from the Tibetan Plateau and flow from north to south in a parallel drainage pattern. The geological conditions of many ore-forming zones including the stratum, the structure and magma activities have indicated that there is a preferred environment for ore formation and a great number of metal ores in different sizes have been discovered in the west part of the Kunlun orogenic zone[17] such as the Zankan iron deposit, the Laobing iron deposit, the Datong iron deposit, the Kekuxilik Pb–Zn deposit, the Huangyangling Sb deposit, the Heiqia iron deposit and Sazigou copper deposit [18] etc. These ore deposits and mineralization points are mainly distributed along the ore-forming belts, which can be further divided into seven sub-metallogenic belts and eighteen mineralization places [19]. The west Kunlun Mountains are one of the best regions for locating large and super-large scale of ore deposits in China.

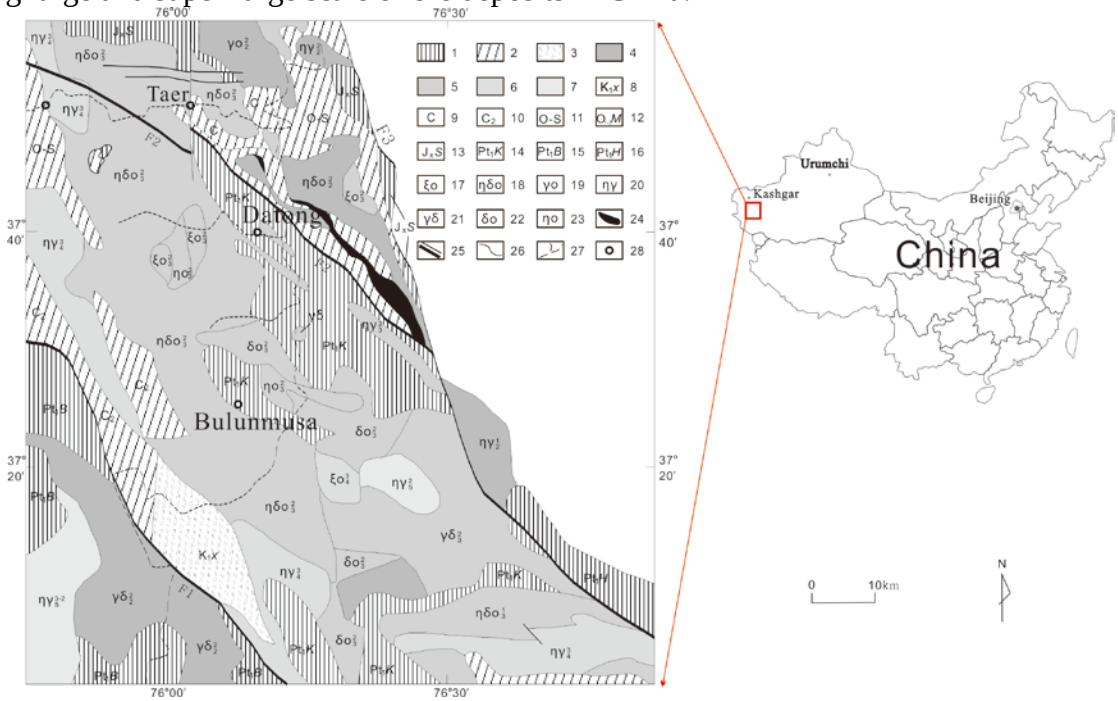

Figure 1 Geological sketch map of study area

(1-Precambrian strata； 2-Paleozoic strata； 3-Mesozoic strata； 4-Proterozoic granitoids； 5-Caledonian granitoids；6-Hercynian granite；7-Yanshan period granite；8-Xiadilafu group；9-Carboniferous； 10-Middle Carboniferous； 11-Ordovician-Silurian； 12-Malieziken Group； 13-Sangzhutage Group；14-Kulangnagu Group；15-Bulunkuole Group；16-Heluositan Guoup；17-Quartz syenite ； 18-Quartz monzobiorite ； 19-Tonalite ； 20-Monzonitic granite ； 21-Granodiorite； 22-Quartz diorite； 23-Quartz monzonite； 24-ultrabasic rocks； 25-Fault； 26-Geological boundary；27-Rivers；28-Towns；F1-Kang Xiwa fault zone；F2-Ke Gang fault zone；F3-Kuslap fault zone)

Based on the regional geology and classification of ore deposits in the study area, Datong iron deposits were selected for this study. This study is concerned with an application of WorldView-2 multispectral data and Spectral Matched Filtering method for iron oxides mapping in Datong

potential iron mineralization zone. The objective of this research was to map surface iron oxide minerals using endmenber spectrum from USGS spectral library. Then, field works were carried out to check whether the predicted iron oxide regons were the potential iron mineralization zones.

3. Materials and Methods

WorldView-2 multispectral data acquired during May 23, 2010 was used in this study. It is the first commercial, high-resolution satellite successfully launched on October 8, 2009 by DigitalGlobe. With the launch of the WorldView-2 satellite, for the first time ever, a high spatial resolution space-borne sensor with eight spectral bands raging from blue to the near infrared parts of the electromagnetic spectrum has been operating [20]. According to its manufacturer, the additional Coastal Blue (400-450 nm), Yellow (585-625 nm), Red-Edge (705-745 nm), and NearIR-2 (860-1040 nm) bands can provide an increase of up to 30% in the classification accuracy, if compared to analyses performed with only the four multispectral bands also available in sensors like the GeoEye-1, Ikonos or the QuickBird-2 [21]. Due to its greater spatial resolution and higher spectral fidelity, WorldView-2 images could proviede higher potential not only for bathymetric studies and vegetation analysis, but also for the mapping of land resources with similar spectral properties, such as iron oxide minerals. The sensor specification of WorldView-2 is given in Table 1.

Table 1 Specification of WorldView-2 sensors

Specifications	Multispectral band informations
Spatial resolution	1.84 [m]
Radiometry	12 bits
Spectral bands [nm]	1. Coastal Blue [400 to 450 nm]
	2. Blue [450 to 510 nm]
	3. Green [510 to 580 nm]
	4. Yellow [585 to 625 nm]
	5. Red [630 to 690 nm]
	6. Red-Edge [705 to 745 nm]
	7. NIR-1 [770 to 895 nm]
	8. NIR-2 [860 to 1040 nm]]

The WorldView-2 data were geometrically corrcted by picking ground control points and using a second-degree polynomial warp with nearest neighbor resampling. The data were processed using FLAASH atmospheric correction software to produce the reflectance data. There are several atmospheic correction algorithms for retrieving surface reflectance from imaging spectometer data, such as Atmosphere Correction Now [22], High-accuracy Atmospheric Correction [23], Imaging Spectrometer Data Analysis System [24] , and a series of Atomospheric and Topographic Correction codes, Fast Line of-sight Atmospheric Analysis of Spectral Hypercubes (FLAASH). FLAASH is a MODTRAN-based atmospheric correction software developed jointly by the Air Force Phillips Laboratory, Hamscon AFB and Spectral Sciences, Inc. [25]. The spectral radiance L* at a sensor pixel maybe parameterized as [26]:

$$L^* = \frac{A\rho}{1 - \rho_e S} + \frac{B\rho_e}{1 - \rho_e S} + L_a^* \qquad (1)$$

Where ρ is the pixel surface reflectance, ρe is an average surface reflectance for the surrounding region, S is the spherical albedo of the atmosphere, L^*_a is the radiance backscattered by the atmosphere without reaching the surface, and A and B are surface independent coefficients that vary with atmospheric and geometric conditions.

Spectral Matched Filtering (SMF) was used to find the abundances of user-defined end member using a partial unmixing[27]:

$SMF(x)=(t-m)^{T}S^{-1}(x-m)$ (2)

Where t, x, m and S are target vector, sample vector, background mean and background covariance, respectively (). The resulting SMF(x) is thresholded to control the false alarm rate.

This is a rapid method for detecting specific materials based on spectral reflectance curves matching with the images, and it constrrains the response of the desired end member and minimizing the response of the background [28]. The results of the SMF appear as a gray-scale image, and have values that range from 0 to 1, where 0 represents a non-match to the end member spectra and 1 represents a perfect match. Thresholds can then be identified to create binary maps from the fraction maps to show areas with relatively good matches to the end member spectra. Unlike linear unmixing, SMF does not require knowledge of all the end members within the scene. Thus in areas of highly mixed rocks, where identification of all the end members is difficult, SMF may be a better choice for identification certain minerals such as iron oxide minerals [29].

Weathered or altered iron oxides are detected in the visible to near-infrared region (VNIR) with silicon sensing technology. In the VNIR, materials containing Fe2+ and Fe3+ produce identifiable spectra. Wavelength-specific absorption of electromagnetic radiation yields diagnostic reflectance spectra for many minerals in the visible to short-wave infrared range [2]. There are variations in iron oxide species; for example, limonite is more abundant in stable landscapes, whereas goethite is more common in active erosional or depositional environments. Limonite is a secondary iron mineral and forms in all types of hydrothermal replacement deposits. The reflectance spectra of the iron oxide minerals involved in the present study [gothite and limonite] are shown in Figure 2a. Iron oxide minerals are dominated by the conduction band edge in the visible part of the spectrum. It is this well-resolved absorption edge between 0.5 μm and 0.6 μm which accounts for the transopaque behavior of iron oxide minerals, imparting strong yellow, brown, and red colours [30]. The continuum removed data of the reflectance spectra are shown in Figure 2b, and it clearly reveals the main absorption peak between 0.5 μm and 0.6 μm of gothite and limonite. And it indicates the iron oxide minerals have the similar absorption feature. So, the gothite reflectance data from USGS spectral library that resampled on WorldView-2 bands were chosen as the iron oxide endmember.

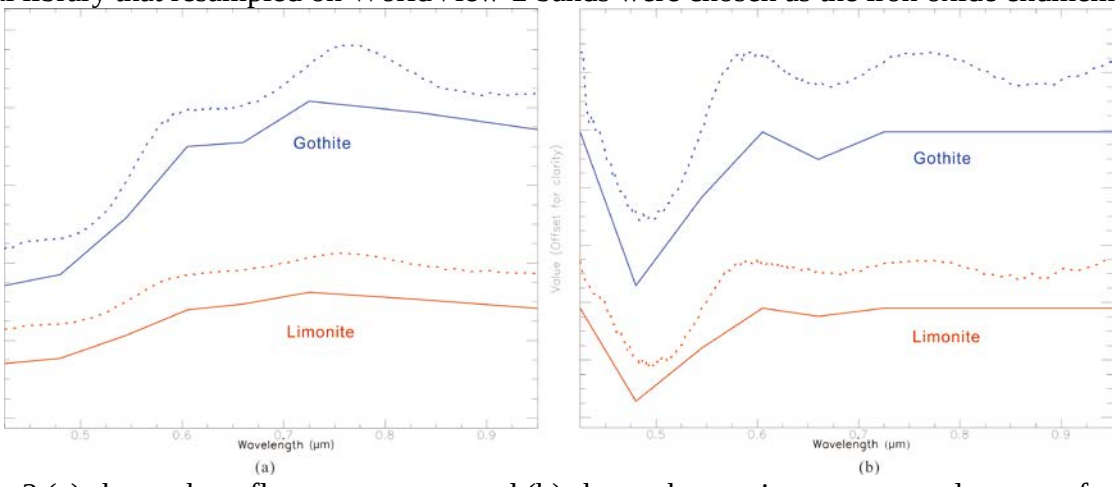

Figure 2 (a) shows the reflectance curves, and (b) shows the continuum removed curves of gothite (blue) and limonite (red). The dotted lines were collected from USGS spectral library and the solid line were resampled on WorldView-2 bands.

4. Results and Discussion

Figure 3 shows the SMF map produced using WorldView-2 data, and the gothite spectrum was chosen from the USGS spectral library as an endmember. The lighter area on these images show better matches to the gothite spectra while the darker area reveal poor matching. In order to suppress the noise of the SMF map, the result has been smoothed by applying a 3×3 mean filter.

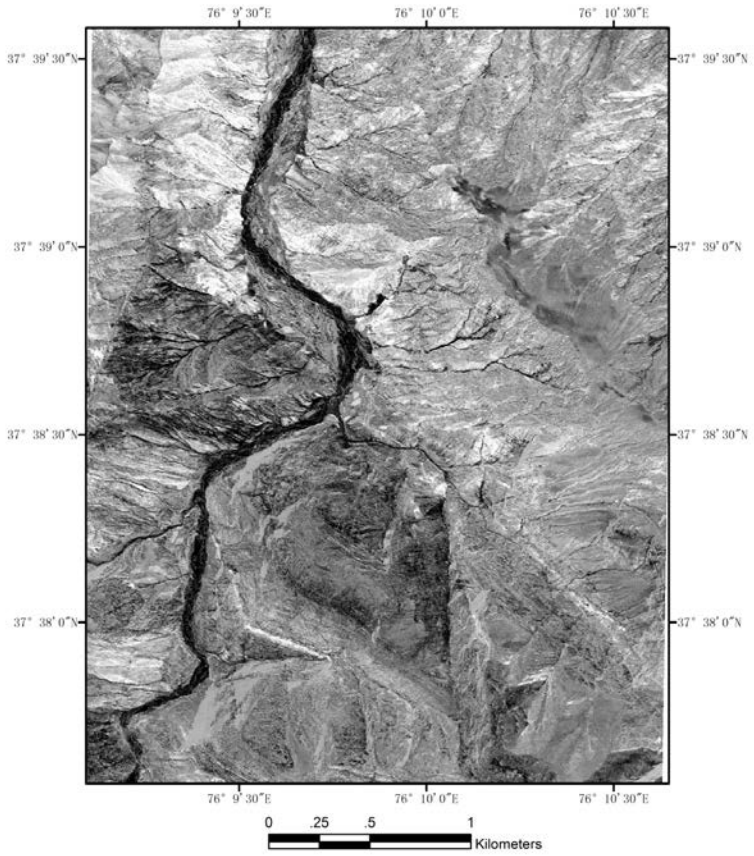

Figure 3 Matched filtering [MF] map of iron oxide minerals

Figure 4 contains a iron oxide distribution map that was produced by thresholding the SMF map. A threshold of >2 standard deviations was used to create the iron oxide distribution map that indicate a high accuracy matched to the gothite endmember. Thus much of the area remains unclassified. The SMF processing techniques could clearly show the distribution of iron oxide minerals in the study area [31].

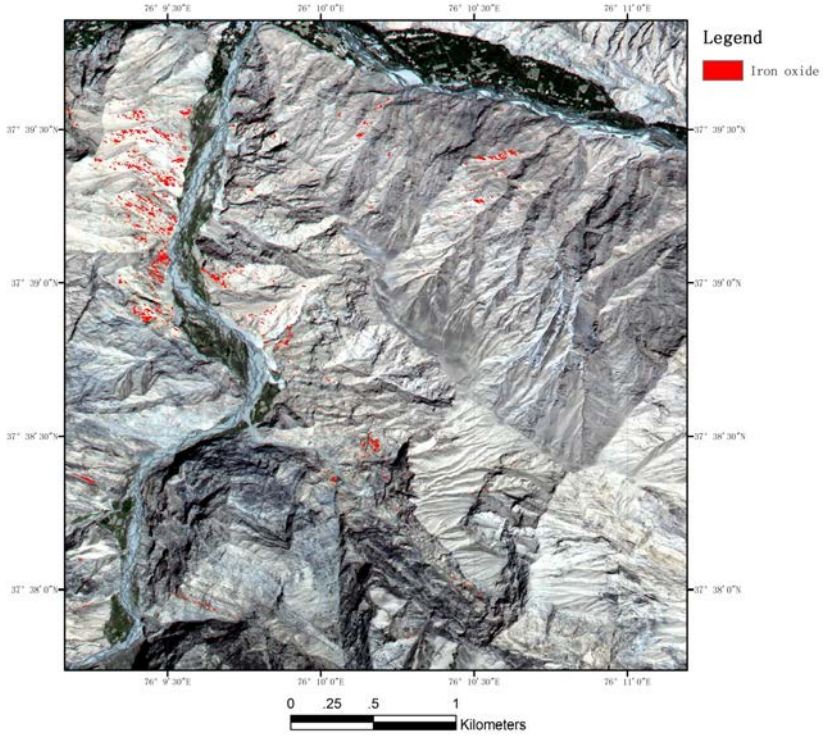

Figure 4 Distribution map of iron oxide minerals

To assess how well the SMF method predict the iron oxide minerals, a comparison plot was performed. Figure 5 shows the similarity between the gothite spectrum data from USGS spectral library and the spectrum of iron oxide from image. And it indicates that in general the SMF method provide an accurate result of the iron oxide minerals mapping. The spectra collected on image and the spectra [gothite and limonite] from USGS spectral library have the similar feature on the plot.

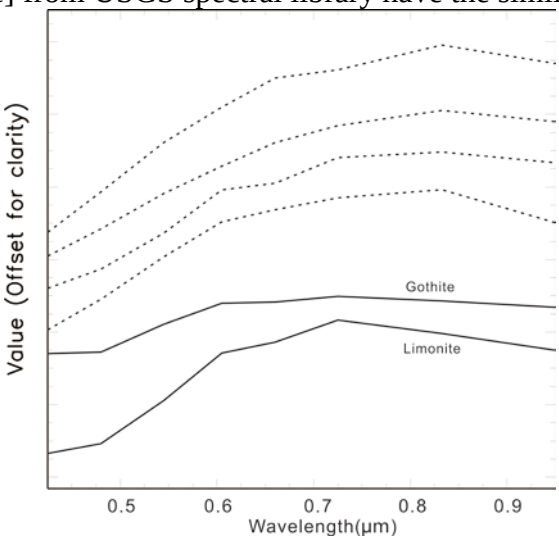

Figure 5 The comparison plot (The dotted lines were collected on image, and the solid lines were from USGS spectral library)

According to the result of SMF mapping, a field reconnaissance was carried out to check the mapping accuracy. During the field work, two potential iron mineralization zones were found in the study area [Figure 6]. Seven samples for laboratory studies were collected through a systemaic rock sampling in the two potential iron mineralization zones. The field photographs of the iron mineralization zones are shown in Figure 7. ICP-AES was used for the simultaneous determination of the total content of Fe in the samples collected from the two potential iron mineralization zones. All samples were paformed iron concentration, and four were over 10 percent. Table 2 shows the Fe content ratios of the seven samples.

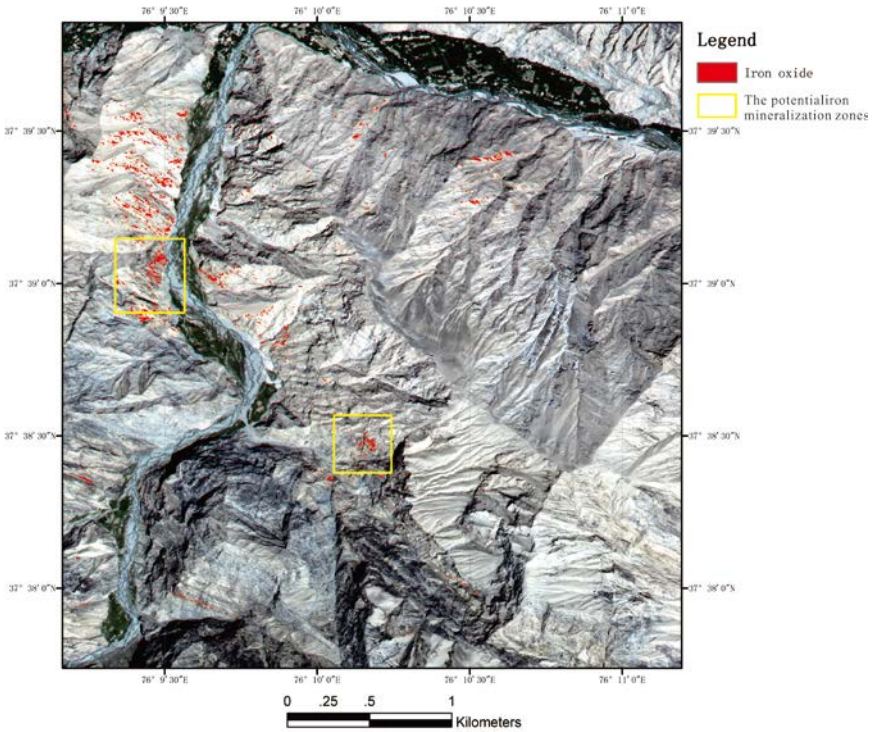

Figure 6 The location of two potential iron mineralization zones

Figure 7 The field photographs of the iron mineralization zones
(The brown part is mainly iron oxide minerals, the dark part is mainly magnetite)

Table 2 Iron content of ICP-AES analysis

Sample No.	XKY012	XKY014	XKY034	XKY035	XKY037	XKY042	XKY049
Fe content[%]	10.40	5.04	10.52	18.17	17.73	5.42	3.86

According to previous remote sensing and geology studies in the study area, the applied SMF technique in the present study efficiently revealed the iron oxide minerals around potential iron mineralization zones and identified new prospects. Results indicate that the SMF technique has a great ability to obtain comprehensive and significant information for the reconnaissance stages of iron deposits exploration in a regional scale. This approach in the image processing technique can be extrapolated to virgin regions for exploring of the new prospect of high-potential iron mineralization zones of the West Kunlun and other arid and semi-arid regions of the Earth.

5. Conclusions

The results from this study indicate that Spectral Matched Filtering technique used in WorldView-2 multispectral data holds promise for the identification of potential iron mineralization zones in China's West Kunlun area. The method presented in this paper for producing an iron oxide distribution map differ from other methods that are used mapping all the end members on the earth surface. It just need to map the key end menbers that perform high correlation with the deposits, and make the ore related minerals mapping quite simple and more efficiency.

Acknowledgments

Authors are thankful to DigitalGlobe for providing test data of WorldView-2 for this study, and thankful to the Key Lab. For the Study of Focused Magmatism and Giant ore Deposits, Ministry of Land and Resources, China for their experiment of ICP-AES. They are also thankeful to editor-in-chief for their valuable guidance and suggestions in improving the manuscript. And thanks for the hard work of corresponding author Jianqiang Li and other authors.

References and Notes

[1] R. N. Clark, Spectroscopy of rocks and minerals, and principles of spectroscopy, remote sensing for the Earth sciences, In Manual of remote sensing. 3rd editon, 3 (1999) 3-58.

[2] G. R. Hunt, Spectral signatures of particulate minerals in the visible and near0infrared, Geophysics, 42 (1977) 501-513.

[3] A. F. H. Goetz, G. Vane, G. J. Solomon, B. N. Rock, Imaging spectrometry for Earth remote sensing, Science, 228 (1985) 1147-1153.

[4] R. N. Clark, J. Boardman, J. Mustard, F. Kruse, C. Ong, C. Pieters, G. Swayze, Mineral mapping and applications of imaging spectroscopy, Proceedings, IGARSS 2006,31 July-4 August 2006, Denver, Colorado, 4 (2006) 1986-1989.

[5] J. C. Harsanyi and C. I. Chang, Hyperspectral image classification and dimensionality reduction: an orthogonal subspace projection approach, IEEE Trans. Geosci. Remote Sensing, 32 (1994) 779-785.

[6] Q. S. Chen, M. Defrise, F. Deconinck, Symmetric phase-only matched filtering of Fourier-Mellin transforms for image registration and recognition, IEEE Transactions on Pattern Analysis and Machine Intelligence, 16 (1994) 1156-1168.

[7] A. P. Williams, E. R. Hunt, Estimation of leafy spurge cover from hyperspectral imagery using mixture tuned matched filteing, Remote Sensing of Enviroment, 82 (2002) 446-456.

[8] W. A. Marcus, D. J. Legleiter, R. J. Aspinall, J. W. Boardman, R. L. Crabtree, High spatial resolution hyperspectral mapping of in-stream habitats, depths, and woody debris in mountain strems, Geomorphology, 55 (2003) 363-380.

[9] H. Kwon, N. M. Nasrabadi, Hyperspectral target detection using kernel spectral matched filter, Computer Vision and Pattern Recognition Workshop, June, 2004. 127-132,.

[10] C. I. Chang, Least Squares subspace projection approach to mixed pixel classification for hyperspectral images, IEEE Transactions on Geoscience and Remote Sensing, 36 (1998), 898-912.

[11] A. Ifarraguerri, Multispectral and hyperspectral image analysis with convex cones, IEEE Transactions on Geoscience and Remote Sensing, 37 (1999) 756-770.

[12] D. Manolakis, D. Marden, J. Kerekes, G. Shaw, On the statistics of hyperspectral imaging data, Algorithms for Multispectral, Hyperspectral, and Ultraspectral Imagery VII, 4381 (2001) 308-316.

[13] C. C. Funk, J. Theiler, D. A. Roberts, C. C. Borel, Clustering to improve matched filer detectiof weak gas plumes in hyperspectral thermal imagery, IEEE Transactions on Geoscience and Remote Sensing, 39 (2001) 1410-1420.

[14] Z. W. Zhang, J. T. Peng, J. F. Xiao, X. Q. Zhu, N. P. Shen, Z. S. Zhang, F. H. Yu, Regional metallotectonics of the lead-zinc deposits zone in southestern margin of the Tarim plate, Bull. Mineral Petrol. Geochem. 28 (2010) 42-43.

[15] Z. W. Zhang, J. T. Peng, J. F. Xiao, X. Q. Zhu, N. Q. Shen, Z. S. Zhang, F. H. You, Regional metallotectonics of the lead-zinc deposits zone in southwest margin of the Tarim plate, Bull. Mineral Petrol. Geochem., 28 (2009) 318-329.

[16] Y. G. Dong, K. Y. Guo, S. B. Liao, H. L. Xiao, T. Wang, Geological and geochemical characteristics of the Kekuxilik lead-zinc ore deposit, west Kunlun, Xinjiang Acta Geological Sinica, 88 (2006) 1730-1738.

[17] Q. Z. Jia, Massive sulfide copper deposits of West Kunlun, Xinjiang, Geological Publishing House, Beijing, 130, 1999.

[18] Y. G. Dong, K. Y. Guo, H. L. Xiao, C. L. Zhang, Y. Zhao, Ore-forming conditions and prospecting in the west Kunlun area, Xinjiang, China, Acta Geologica Sinica-English Edition, 78 (2004) 345-351.

[19] Z. W. Zhang, G. D. Zheng, K. Shozugawa, M. Matsuo, Y. D. Zhao, Iron and sulfur speciation in some sedimentary-transformation-type of lead-zinc deposits in West Kunlun Lead-Zinc ore deposit zone, Northwest China, Journal of Radioanalytical and Nuclear Chemistry, 295(2013) 83-90.

[20] T. Novack, T. Esch, H. Kux, U. Stilla, Machine learning comparison between WorldView-2 and QuikBird-2-simulated imagery regarding object-based urban land cover classification, Remote Sensing, 3 (2011) 2263-2282.

[21] DigitalGlobe, The benefits of the 8 spectral bands of WorldView-2, Available online: http://www.digitalglobe.com/index.php/88/WorldView-2, 2010.

[22] F. A. Kruse, Comparison of ATREM, ACORN, and FLAASH atmospheric corrections using low-altitude AVIRIS data of Boulder, In: Summaries of 13th JPL Airborne Geoscience Workshop, Jet Propulsion Lab, 2004.

[23] Z. Qu, B. C. Kindel, A. F. H. Goetz, The high accuracy atmospheric correction for hyperspectral data [HATCH] model, IEEE Transactions on Geoscience and Remote Sensing, 41 (2003) 1223-1231.

[24] K. Staenz, T. Szeredi, J. Schwarz, ISDAS-a system for processing/analyzing hyperspectral data, Can. J. Remote Sens., 24 (1998) 99-113.

[25] J. Cui, B. Yan, R. Wang, F. Tian, Y. Zhao, D. Liu, S. Yang, W. Shen, Regional-scale mineral mapping using ASTER VNIR/SWIR data and validation of reflectance and mineral map producets using airborne hyperspectral CASI/SASI data, International Journal of Applied Earth Observation and Geoinformation, 33 (2014) 127-141.

[26] A. Berk, S. M. Adler-Golden, A. J. Ratkowski, et al., Exploiting MODTRAN Radiation Transport for Atmospheric Correction: The FLAASH Algorithm, Information Fusion Proceedings of the Fifth International Conference, 2 (2002) 798-803.

[27] B. Sadeghi, M. Khalajmasoumi, P. Afzal, P. Moarefvand, A. B. Yasrebi, A. Wetherelt, P. Foster, A. Ziazarifi, Using ETM+ and ASTER sensors to identify iron occureences in the Esfordi 1:100000 mapping sheet of central Iran, Journal of African Earth Sciences, 85 (2013) 103-114.

[28] S.Gabr, A. Ghulam, T. Kusky, Detecting areas of high-potential gold mineralization using ASTER data, Ore Geology Reviews, 38 (2010) 59-69.

[29] J. R. Harris, D. Rogge, R. Hitohcock, O. Ljewliw, D. Wright, Mapping lithology in Canada's Arctic: application of hyperspectral data using the minimum noise fraction transformation and matched filtering, Can. J. Earth Sci., 42 (2005) 2173-2193.

[30] K. White, J. Walden, N. Drake, F. Eckardt, and J. Settle, Mapping the iron oxide content of dune sands, Namib Sand Sea, Namibia, using Landsat thematic mapper data, Remote Sens. Environ., vol. 62 (1997) 30-39.

[31] A. B. Pour, M. Hashim, Identification of hydrothermal alteration minerals for exploring of porphyry copper deposit using ASTER data, SE Iran, Journal of Asian Earth Sciences, 42 (2011) 1309-1323.